NAM

Advanced modelling of URM buildings in support of fragility and consequence functions derivation

Using the Applied Element Method to model the collapse shake-table testing of a terraced house roof substructure

Daniele Malomo and Rui Pinho

Mosayk

Date October 2017

Editors Jan van Elk & Dirk Doornhof

General Introduction

Many of the buildings in the Groningen field area are terraced unreinforced masonry buildings. A program to assess the response of these building to earthquakes was therefore initiated. This program built on the experimental and modelling program into the properties of URM building materials, wall elements and wall units.

A typical Groningen terraced house built using materials from the Groningen area by builders from the Groningen area, was tested at the shake-table of Eucentre in Pavia, Italy (Ref. 1). Although the building was at the end of this test program seriously damaged, the building had not collapsed. This left questions on the remaining capacity of the structure and its ability to resist larger seismic movements before (partially) collapsing. The test in Eucentre was therefore followed-up with further tests at the laboratory of LNEC in Lisbon, Portugal (Ref. 2 to 6). Here the upper floors of the building tested in Eucentre were re-built in the LNEC laboratory and subjected to movements measured at the base of the upper floors in Eucentre.

Additionally, the roof structure was tested individually. This report shows the results of modelling of the test in LNEC for the roof structure of the terraced building obtained by Mosayk using Extreme Loading for Structures (ELS), a commercial structural analysis software based on the Applied Element Method (AEM) after such tests, describing also the calibration process of the AEM numerical model.

References

1. Eucentre Shake-table Test of Terraced House Modelling Predictions and Analysis Cross Validation, staff from ARUP, Eucentre (Pavia) and TU Delft, November 2015 [this document also includes; (1) Instruments full-scale test-house Eucentre Laboratory, (2) Protocol for Shaking Table Test on Full Scale Building (Eucentre) V_1, and (3) Selection of Acceleration Time-Series for Shake Table Testing of Groningen Masonry Building at the EUCENTRE, Pavia, all three by staff from Eucentre (Pavia)],
2. Collapse shake-table testing of terraced house (LNEC-BUILD1), Eucentre and LNEC (U. Tomassetti, A. A. Correia, F. Graziotti, A.I. Marques, M. Mandirola, P.X. Candeias), 1st September 2017.
3. LNEC-BUILD1: Modelling predictions and analysis cross-validation, ARUP, TU Delft, Eucentre and Mosayk (several staff members from all four institutions), 8th September 2017.
4. Using the Applied Element Method to model the collapse shake-table testing of a URM cavity wall structure (LNEC-BUILD1), Mosayk (D. Malomo, R. Pinho), 31st October 2017.
5. Shake-table test up to collapse on a roof substructure of a Dutch terraced house (LNEC-BUILD2), Eucentre and LNEC (A.A. Correia, A.I. Marques, V. Bernardo, L. Grottoli, U. Tomassetti, F. Graziotti), 31st October 2017.
6. Using the Applied Element Method to model the collapse shake-table testing of a terraced house URM cavity wall structure (LNEC-BUILD2), Mosayk (D. Malomo, R. Pinho), 31st October 2017.

NAM

Title	**Using the Applied Element Method to model the collapse shake-table testing of a terraced house roof substructure**		**Date**	October 2017
			Initiator	NAM
Autor(s)	**Daniele Malomo and Rui Pinho**	**Editors**	Jan van Elk and Dirk Doornhof	
Organisation	**Mosayk**	**Organisation**	NAM	
Place in the Study and Data Acquisition Plan	Study Theme: Development of Fragility Curves Comment: Many of the buildings in the Groningen field area are terraced unreinforced masonry buildings. A program to assess the response of these building to earthquakes was therefore initiated. This program built on the experimental and modelling program into the properties of URM building materials, wall elements and wall units. A typical Groningen terraced house built using materials from the Groningen area by builders from the Groningen area, was tested at the shake-table of Eucentre in Pavia, Italy (Ref. 1). Although the building was at the end of this test program seriously damaged, the building had not collapsed. This left questions on the remaining capacity of the structure and its ability to resist larger seismic movements before (partially) collapsing. The test in Eucentre was therefore followed-up with further tests at the laboratory of LNEC in Lisbon, Portugal (Ref. 2 to 6). Here the upper floors of the building tested in Eucentre were re-built in the LNEC laboratory and subjected to movements measured at the base of the upper floors in Eucentre. Additionally, the roof structure was tested individually. This report shows the results of modelling of the test in LNEC for the roof structure of the terraced building obtained by Mosayk using Extreme Loading for Structures (ELS), a commercial structural analysis software based on the Applied Element Method (AEM) after such tests, describing also the calibration process of the AEM numerical model.			
Directliy linked research	(1) Building Material properties (2) Shake table tests (3) Seismic Response of Buildings (URM and non-URM) (4) Risk Assessment			
Used data	Full experimental and Modelling program into seismic response URM & non-URM buildings.			
Associated organisation	NAM			
Assurance	Independent Assurance Panel			

D7

DELIVERABLE

Project Information

Project Title:	**Advanced modelling of URM buildings in support of fragility/consequence functions derivation**
Project Start:	May 2016
Duration:	20 months
Technical Point of Contact:	Rui Pinho
Administrative Point of Contact:	Roberto Nascimbene

Deliverable Information

Deliverable Title:	**Using the Applied Element Method to model the collapse shake-table testing of a terraced house roof substructure**
Data of Issue:	31st October 2017
Author:	Daniele Malomo
Reviewer:	Rui Pinho

REVISION: **v1**

Table of Contents

Executive Summary

A full-scale component shake-table specimen (LNEC-BUILD2) was tested in 2017 at the shake-table of the Laboratório Nacional de Engenharia Civil (LNEC - Lisbon, Portugal) under the coordination of the European Centre of Training and Research in Earthquake Engineering (Eucentre - Pavia, Italy). The test was carried out within the framework of the research programme on hazard and risk of induced seismicity in the Groningen region, sponsored by the Nederlandse Aardolie Maatschappij BV (NAM).

In tandem with such experimental endeavour, an informal blind-prediction modelling exercise was also undertaken, involving two different modelling teams, each of which employing diverse structural modelling strategies and tools. Mosayk was one of such two teams, modelling the test specimen using Extreme Loading for Structures (ELS), a commercial structural analysis software based on the Applied Element Method (AEM).

This report shows the results obtained by Mosayk both before (blind prediction) as well as after (calibrated post-diction) the test, describing also the calibration process of the AEM numerical model. It is shown that the (post-test) model is able to produce response estimations that are reasonably close to the experimentally observed behaviour of the tested full-scale specimen, and also how an error in the definition of the foundation boundary conditions of the blind prediction model explains the failure of the latter in adequately predicting the response of LNEC-BUILD2.

Nomenclature

Symbol	Description
ρ	Mass density [kg/m^3]
E	Masonry Young's modulus [MPa]
E_{mo}	Mortar Young's modulus [MPa]
E_u	Unit Young's modulus [MPa]
ν	Poisson's ratio of masonry
f_m	Masonry compressive strength [MPa]
f_w	Flexural bond strength of mortar joints [MPa]
f_{v0}	Masonry (bed joint) initial shear strength (cohesion) [MPa]
μ	Masonry (bed joint) shear friction coefficient

1 Introduction

1.1 Scope

The full-scale test specimen LNEC-BUILD2 built in the LNEC laboratory in Lisbon is the roof substructure of the EUC-BUILD1 specimen tested in the Eucentre laboratory in 2015 (see report by Graziotti et al., 2015). For this reason, the seismic input introduced at the base of LNEC-BUILD2 specimen corresponded to the second floor accelerations that had been recorded during the EUC-BUILD1 test. Further details can be found in the corresponding test report (Correia et al., 2017).

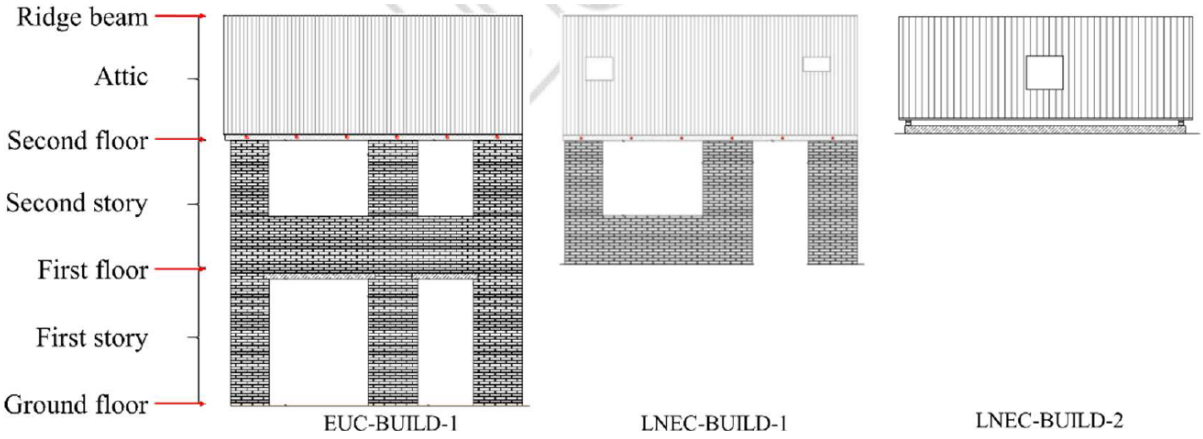

Figure 1 Comparison of EUC-BUILD1, LNEC-BUILD1 and LNEC-BUILD2 test specimens (from Arup, 2017)

The aim of this test was to enhance further the knowledge of the seismic response of a flexible roof diaphragm + gable walls substructure up to collapse, for which reason an incremental shake-table test was performed. Moreover, since no significant damage was detected in the wooden roof structure after the out-of-plane collapse of the gable walls, the former was subjected to quasi-static cyclic testing, so that experimental data useful for the calibration of models of such structural components could be obtained.

An informal blind-prediction modelling exercise was also undertaken, involving two different modelling teams, each of which employing diverse structural modelling strategies and tools. Mosayk was one of such two teams, modelling the test specimen using ELS - Extreme Loading for Structures (ASI, 2017), a commercial structural analysis software based on the Applied Element Method (Meguro and Tagel-Din, 2000, 2001, 2002). This report thus describes such modelling effort by Mosayk.

1.2 Analysis method

According to the Applied Element Method (AEM), a given structure is discretised as a virtual assembly of small rigid units, carrying only mass and damping of the system, connected by linear and nonlinear springs (with normal stiffness k_n and shear stiffness k_s) in which the material properties are lumped. It is noted that, even if the single mesh element is rigid, the behaviour of the whole assembly is deformable. Thus, a masonry wall segment can be represented by means of units (fully rigid or deformable) linked by dimensionless mortar layers (simplified micro-modelling). The theoretical formulation allows reproducing the structural response both in the finite and discrete numerical domains, taking into account contacts and dynamic element

interactions automatically. In addition to the pioneering publications listed above, further details on the AEM formulation may be found in e.g. Mosayk (2016) and Malomo (2018).

1.3 Building substructure

In this sub-section, a summary of the specimen description found in Correia et al. (2017) is briefly reported, for convenience. The LNEC-BUILD2 prototype is a full-scale timber roof with ceramic tiles, supported on URM gable walls and on a RC slab. The prototype was 5.82 m long, 5.46 m wide and 2.45 m high with a total mass of 17.8 tonnes. The East gable wall was composed of load-bearing calcium silicate (CS) bricks, while the West gable wall was composed of two URM leaves: the inner load-bearing leaf was also made of CS bricks and the outer leaf was made of clay bricks without any load-bearing function. The outer leaf was not present in the East façade, simply because the specimen was meant to represent the end-unit of a set of terraced houses.

The entire specimen was supported on a steel foundation with a 0.16 m thick slab fixed to it. Both CS gable walls were supported on the concrete slab, while the outer clay brick wall was built directly from the steel foundation. An air gap of 80 mm was left between the two leaves, as usually seen in common practice. L-shaped steel ties with a diameter of 3.1 mm and a length of 200 mm were inserted in the 10 mm-thick mortar bed-joints during the laying of the bricks, ensuring the connection between the two masonry leaves. In particular, the L-hook side was embedded into the inner CS wall for a length of 70 mm, while the "zigzag" extremity was embedded into the clay masonry for a length of 50 mm.

The two gable walls in the transverse façades supported the roof beams of the 42° pitched timber roof. The timber beams at the slab level, instead, were attached directly to the longitudinal sides of the slab. A rectangular opening of 0.74 m x 0.70 m was left on the North side of the roof, granting access to the interior.

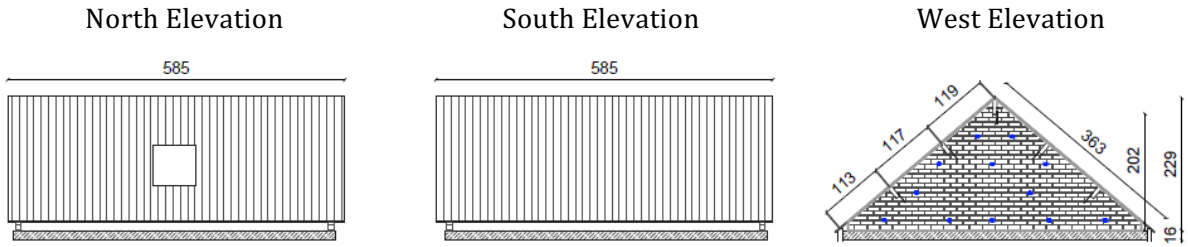

Figure 2 Elevation views of the LNEC-BUILD2 specimen (Correia et al., 2017)

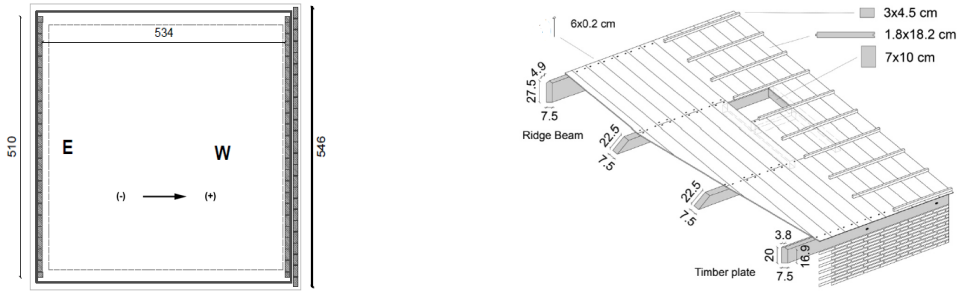

Figure 3 Plan view of the LNEC-BUILD2 specimen (left) and details of roof structure (right) (Correia et al., 2017)

1.4 Mechanical properties of masonry

Both CS and CL masonry components were tested at Eucentre and LNEC in order to characterise the masonry material and obtain the mechanical properties reported in Table 1, below.

Table 1 Masonry material properties

Symbol	**CS**	**CL**
ρ	1800	1839
E	7955[1]	13118[1]
E_{mo}	---	---
E_u	8990	7211
ν	---	---
f_m	9.80	19.39
f_w	0.36	0.25
f_{v0}	0.45	0.41
μ	0.48	0.75

[1] Secant stiffness to 10%fm

1.5 Testing procedure

The specimen was fixed to the shake-table, and the loading protocol showed in Table 2 was subsequently imposed. The records consisted of the measured second floor accelerations from the testing of EUC-BUILD1 with ground motion EQ1-100%, EQ1-150%, EQ2-100%, EQ2-150% and EQ2-200% (Graziotti et al., 2015).

Table 2 LNEC-BUILD2 test sequence

Seq-n°	Test ID	Nom.PGA [g]	Actual PGA [g]	Seq-n°	Test ID	Nom.PGA [g]]	Actual PGA [g]
1	EQ1 @ 50%	0.066	0.074	7	EQ2 @ 200%	0.316	0.487
2	EQ1 @ 100%	0.132	0.143	8	EQ2 @ 300%	0.475	0.668
3	EQ1@150%	0.168	0.170	9	EQ2 @ 400%	0.633	0.935
4	EQ2 @ 50%	0.102	0.106	10	EQ2 @ 500%	0.791	0.955
5	EQ2 @ 100%	0.204	0.207	11	EQ2 @ 100%-C	0.204	0.201
6	EQ2 @ 150%	0.284	0.245	12	EQ2 @ 600%	0.949	1.138

2 Brief Overview of Test Specimen Response

As reported in Correia et al. (2017), the first visible damage associated to shake-table motion was detected during test EQ1@100%. No particular additional damage was visible during tests EQ1@150% and EQ2@50%, although a slight reduction of the specimen's fundamental frequency of vibration was detected.

There was a crack opening at the base the CS East gable wall during test EQ2@100%, with a permanent crack width of around 0.1 mm. Test EQ2@150% caused no new damage on the structure, whilst EQ2@200% only extended already existing cracks.

During test EQ2@300% several new sub-horizontal cracks formed on the East gable wall with their origin at the connection between the CS wall and the roof beams (see Figure 4). Always on the East wall, the main crack opening was a vertical one from the ridge beam downwards, largely contributing to the formation of the collapse mechanism mobilised on the subsequent test, EQ2@600%. The collapse mechanism was then completely formed and that portion of the East gable wall had a full collapse towards the interior of the model.

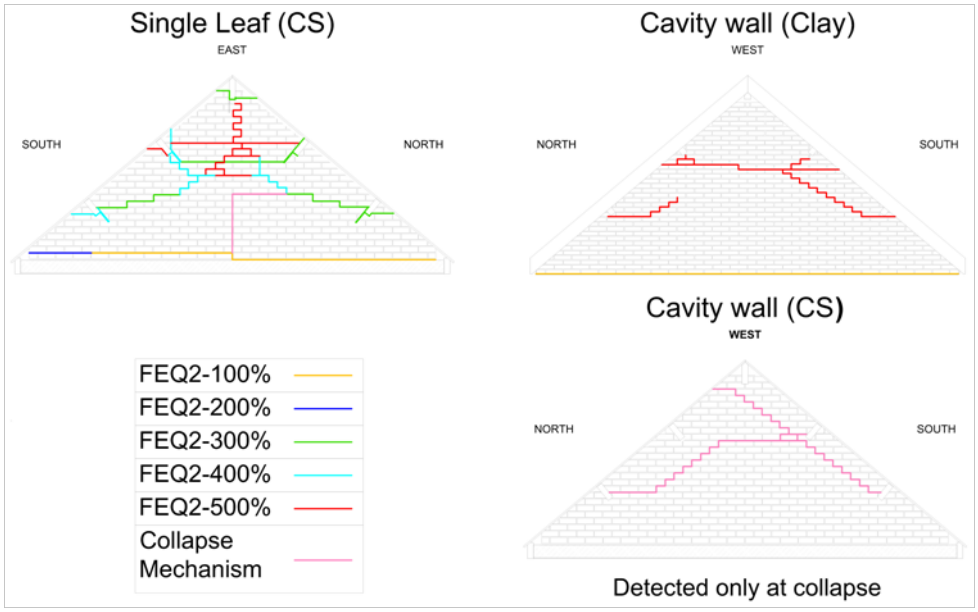

Figure 4 Evolution of the crack pattern in the gable walls along the test stages (Correia et al., 2017)

3 Blind Prediction Modelling

In this section, a brief overview of the results obtained before the test is included. As reported further below, the preliminary numerical model exhibited a very stiff response compared to its experimental counterpart (no significant damage was predicted by the model up to EQ2@600), largely due to a modelling error; the RC slab was not fully fixed to the foundation.

3.1 Preliminary numerical model

The most relevant modelling assumptions related to the numerical model assembled prior to the test (depicted in Figure 4) are briefly summarised in Table 3.

Table 3 Modelling assumptions

Input	Modelling assumption
Boundary condition	Structure connected by mortar interfaces to a fixed slab
Roof diaphragm	Nailed connection between planks and beams modelled as equivalent spring interfaces characterised by an elastic-perfectly-plastic behaviour
Wall ties	Elastic-perfectly-plastic beam elements
RC slab/wall connection	Mortar interface
Connection between roof girders and end/party walls	Mortar interface plus elastic-perfectly plastic L-steel anchors

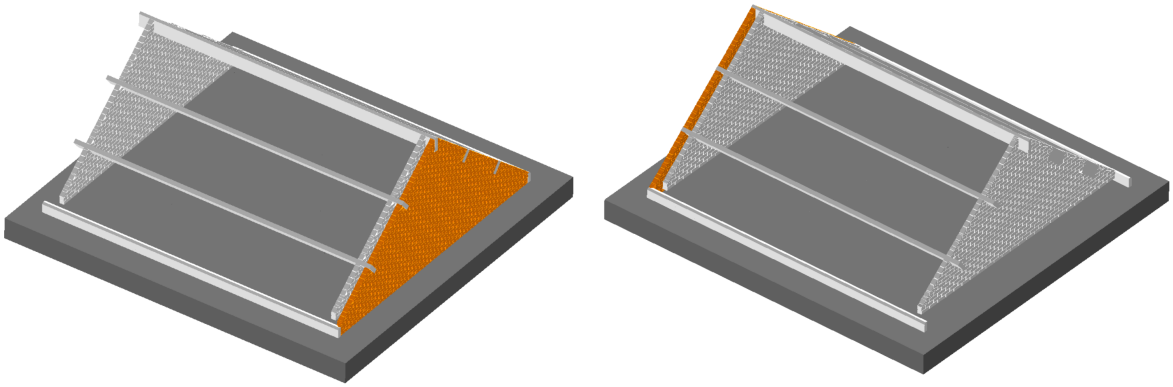

Figure 4 Screenshots of the preliminary numerical model of LNEC-BUILD2

It is also noted that, in order to decrease the computational burden, the bricks were assumed to be rigid and the number of springs was reduced. Thus, mechanisms that involve the deformability of bricks, such as crushing of masonry due to the splitting of the unit, cannot be taken into account, which may result in an underestimation of of energy dissipation. Furthermore, it is noted that the gravity contribution of the roof tiles was modelled through a system of lumped masses shared amongst the elements of the mesh, again with the aim at reducing the calculation steps, resulting in a potentially slightly altered acceleration demand at the roof structure.

3.2 Preliminary material properties

The material properties employed for the LNEC-BUILD1 modelling endeavour (Mosayk, 2017) were considered in the preliminary model employed for the blind prediction.

3.3 Floor hysteresis

Floor hysteresis is defined as the total "base" shear [kN] vs. attic floor horizontal displacement relative to the base [mm]. Grey is experimental and black is numerical.

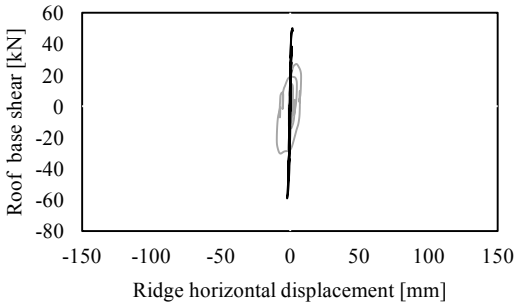

EQ2@200

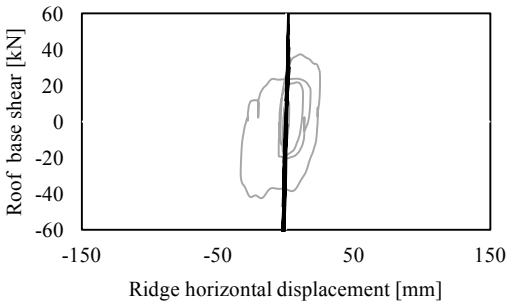

EQ2@300

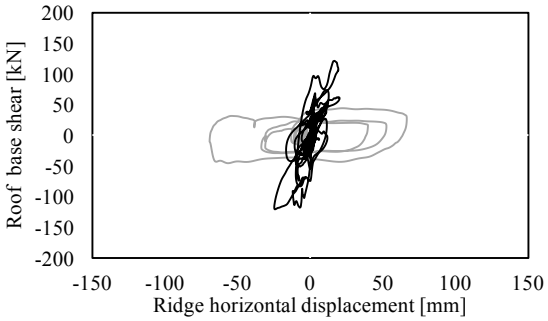

EQ2@400

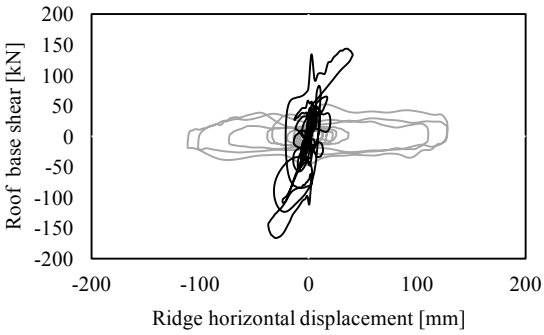

EQ2@500

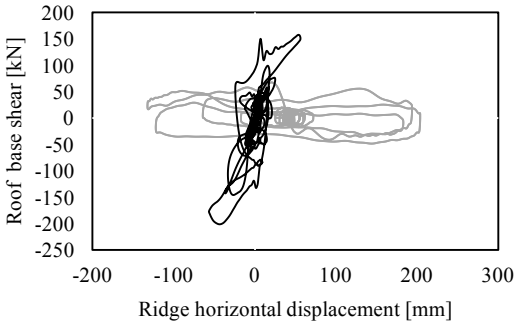

EQ2@600

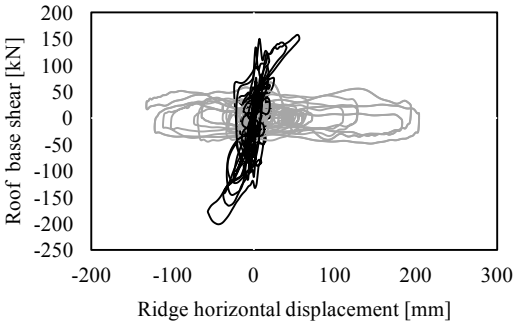

full-cycles hysteresis

As can be readily observed in the plots above, and as mentioned already in this report, the preliminary blind-prediction numerical model exhibited a very stiff response compared to its experimental counterpart. Even if other aspects of the model were also updated (see Section 4.1 below), the main contributor to the ill-performance of the preliminary numerical model was an unintended modelling error, whereby the RC slab was not fully fixed to the foundation.

Whilst it was immediately apparent, ahead of the test execution, that the stiffness values that were being obtained for the specimen were unrealistically high, a decision was made not to error-inspect the model before the test, with a view to assess/confirm the sort of impact that lack of QA scrutiny may have on the outcome of this type of analyses.

4 Post-Test Refined Modelling

4.1 Numerical model

Although the main structure of the previous model was substantially maintained, some improvements were introduced, as summarised in Table 4 and further discussed and detailed in Appendix A. In addition, advantage was also taken of the availability of cyclic test results for the roof alone, which allowed calibrating the model for this component (see Section 5).

Table 4 Modelling assumptions (changes with respect to pre-test model are indicated in bold characters)

Input	Modelling assumption
Boundary condition	Structure connected by mortar interfaces to a fixed slab
Beam/plank connection	**Nailed connection between planks and beams modelled as equivalent spring interfaces characterised by an elastic behaviour**
Plank elements	**Bilinear material with an equivalent shear modulus accounting for flexural and shear deformations and an equivalent yield stress**
Wall ties	Elastic-perfectly-plastic beam elements
RC slab/wall connection	Mortar interface
Connection between roof girders and end/party walls	Mortar interface plus elastic-perfectly plastic L-steel anchors

The post-test roof structure modelling approach is based on the assumption that the overall deformability of the diaphragm can be subdivided into three contributions: the rigid rotation of plank elements due to nail slip and the shear and flexural deformation of the planks, as summarised in Figure 5 below.

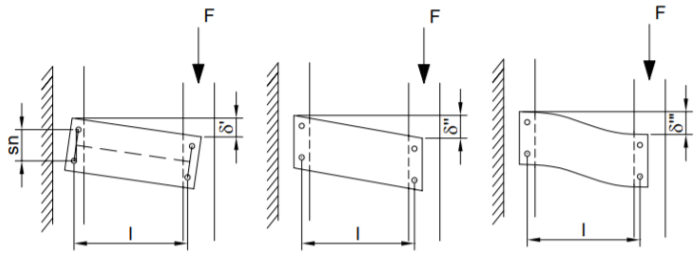

(a) (b) (c)

Figure 5 Rigid rotation of the board due to nails slip; c) board shear deformation; d) board flexural deformation.

The interface between beam and plank element is currently modelled as a linear material, characterised by the same shear stiffness of the nailed connection and allowing the rigid rotation of the planks. The latter, instead, is modelled with bilinear behaviour accounting both for flexural and shear deformation of the flexible diaphragm according to the approach proposed by Brignola et al., (2008). Moreover, an equivalent yield stress was assigned to the plank material accounting for the typical post-peak softening behaviour exhibited by the wooden diaphragms.

4.2 Post-test material properties

In Table 7 and Table 8 below, the final material characterisation test values, as well as values assumed for the post-test modelling for both CS and CL masonry, are reported.

Table 5 CS masonry characterisation test and numerical properties

Symbol	Description	Test value	ELS
ρ	Mass density [kg/m^3]	1800	1835
E	Masonry Young's modulus [MPa]	7955[1]	---
E_{mo}	Mortar Young's modulus [MPa]	---	4537[2]
E_u	Unit Young's modulus [MPa]	8990	8990
ν	Poisson's ratio of masonry	---	0.25
f_m	Masonry compressive strength [MPa]	9.8	---
f_{mo}	Mortar compressive strength [MPa]	6.20	16.3
f_u	Brick compressive strength [MPa]	16.3	16.3
f_w	Flexural bond strength of mortar joints [MPa]	0.36	0.36
f_t	Tensile strength of mortar joints [MPa]	---	0.85[4]
f_{v0}	Masonry (bed joint) initial shear strength (cohesion) [MPa]	0.45	0.45
μ	Masonry (bed joint) shear friction coefficient	0.48	0.48

Table 6 CL masonry characterisation test and numerical properties

Symbol	Description	Test value	ELS
ρ	Mass density [kg/m^3]	1839	1905[2]
E	Masonry Young's modulus [MPa]	13118[1]	---
E_{mo}	Mortar Young's modulus [MPa]	---	3535[2]
E_u	Unit Young's modulus [MPa]	7211	7211
ν	Poisson's ratio of masonry	---	0.25
f_m	Masonry compressive strength [MPa]	19.39	----
f_{mo}	Mortar compressive strength [MPa]	8.34	32.45
f_u	Brick compressive strength [MPa]	32.45	32.45
f_w	Flexural bond strength of mortar joints [MPa]	0.19	0.25
f_t	Tensile strength of mortar joints [MPa]	---	0.98[3]
f_{v0}	Masonry (bed joint) initial shear strength (cohesion) [MPa]	0.41	0.41
μ	Masonry (bed joint) shear friction coefficient	0.75	0.75

[1] Secant stiffness to 33%fm

[2] Inferred by means of empirical formulae (Ciesielski 1999; ICBO 1991; Matysek and Janowski 1996; Brooks and Baker 1998)

[3] Inferred by means of empirical formulae (Kim and Reda Taha, 2014)

Table 7 Plank material modelling parameters

Geometrical parameters		Inferred values	
Board thickness	20 mm	Shear factor	1.2
Board width	180 mm	Shear deformation of the single board	8E-07 m/N
Elastic modulus of wood	12000 MPa	Deformability due to rigid rotation of the board	5.18E-0.5 m/N
Shear modulus of wood	750 MPa	Flexural deformation of the single board	4.16E-06 m/N
Board length	1.8 m	Equivelent shear modulus	120.80 MPa

4.3 Overview of model deformation

The deflected shape prior to collapse, as well as the collapse mechanism itself, are shown in Figure 6 and Figure 7, respectively. The collapse mechanism seems thus to be adequately predicted by the model (further discussion on the model's accuracy can be found in the two subsequent sub-Sections).

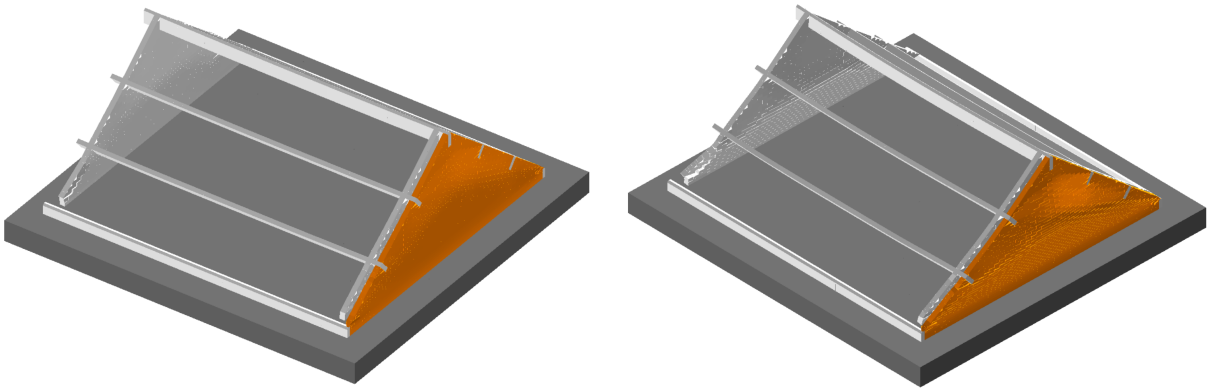

Figure 6 Deflected shapes at maximum excursion prior to collapse

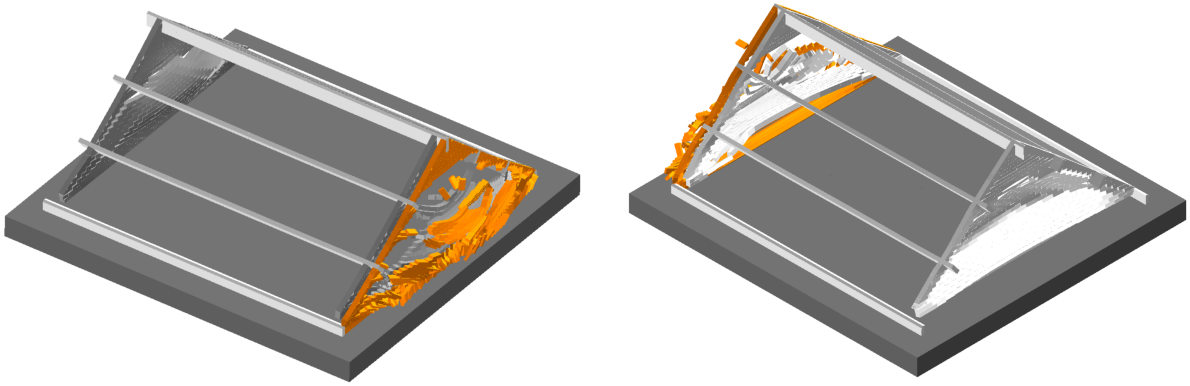

Figure 7 Deflected shapes at maximum excursion prior to collapse

4.4 Floor hysteresis

A comparison between the numerical and experimental hysteretic response in terms of floor displacement (i.e. total "base" shear [kN] vs. attic floor horizontal displacement relative to the base [mm]) is show in the plots below, where grey stands for experimental recordings and black is numerical results.

As can be readily observed, the results are now significantly improved with respect to the previously report blind prediction results, owing to the correct modelling of the foundation boundary conditions and the adjustments introducing in the modelling of the roof structure (see Section 4.1 above).

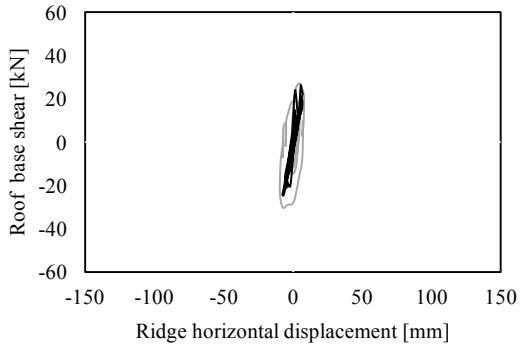

EQ2@200

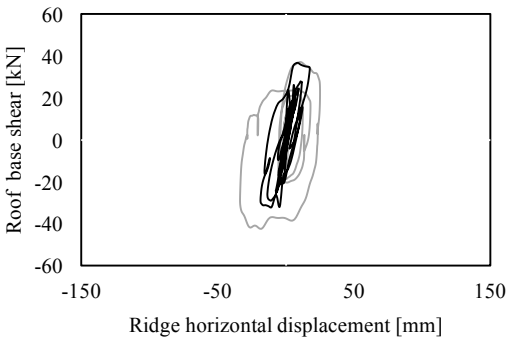

EQ2@300

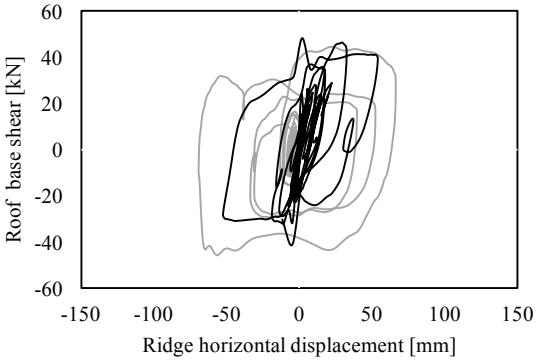

EQ2@400

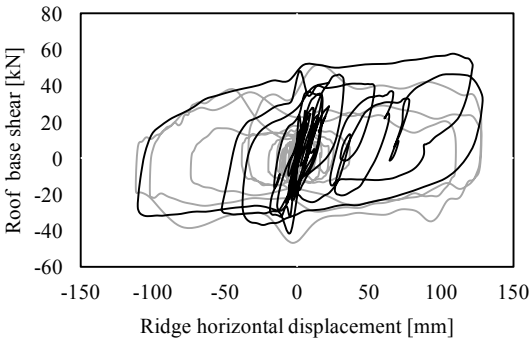

EQ2@500

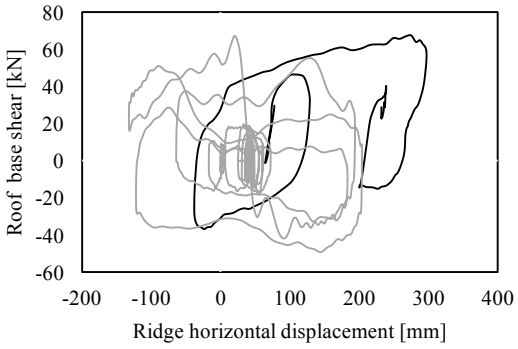

EQ2@600

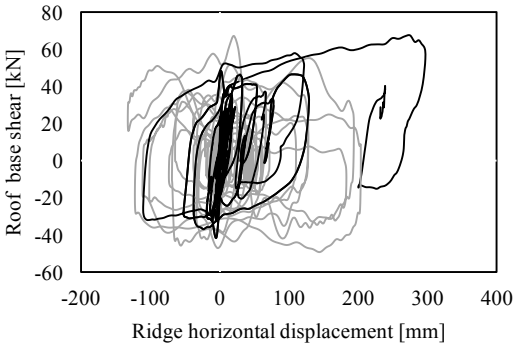

full-cycles hysteresis

4.5 Crack patterns and collapse mechanism

The final damage predictions for each wall (both CS and CL masonry elements) are compared in this sub-Section with their experimental counterparts (varied magnification).

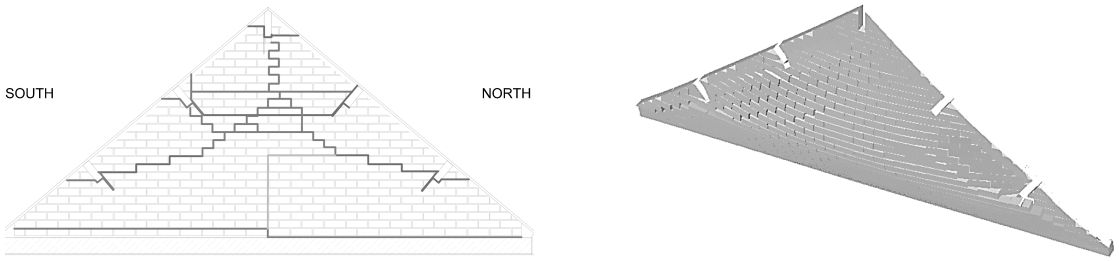

Figure 8 EQ2@500 _ Experimental (left) and numerical (right) damage plot of CS single leaf

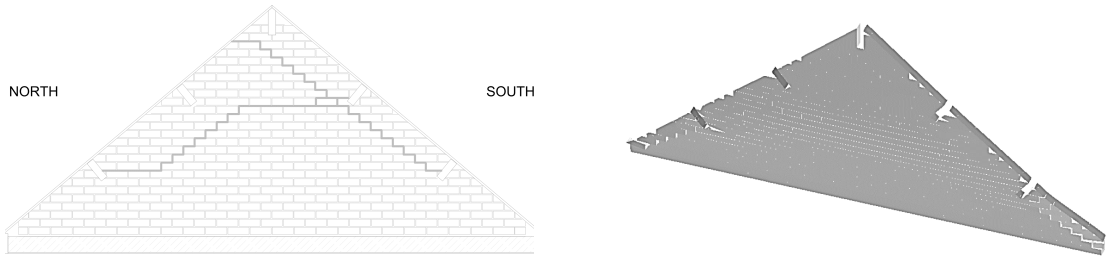

Figure 9 EQ2@600 _ Experimental (left) and numerical (right) damage plot of CS cavity wall prior to collapse

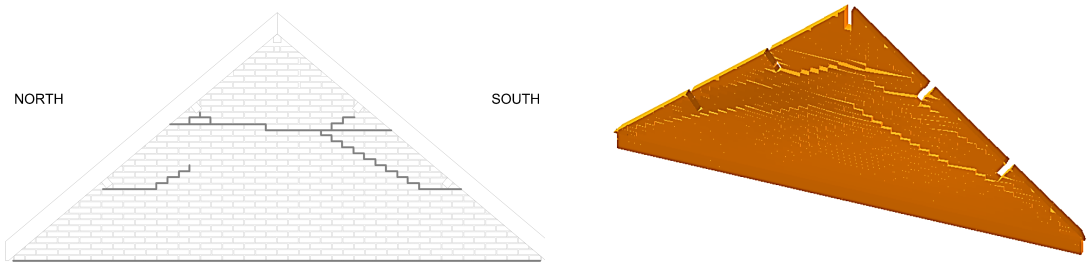

Figure 10 EQ2@600 _ Experimental (left) and numerical (right) damage plot of CL cavity wall prior to collapse

5 Modelling of Roof Cyclic Testing

5.1 Introduction

After the collapse shake-table testing of the complete roof substructure, non-collapsed URM elements were carefully removed and a support system was put in place to allow additional testing on the timber roof; a cyclic pushover was performed in order to further understand the stiffness and hysteretic response of the roof structure.

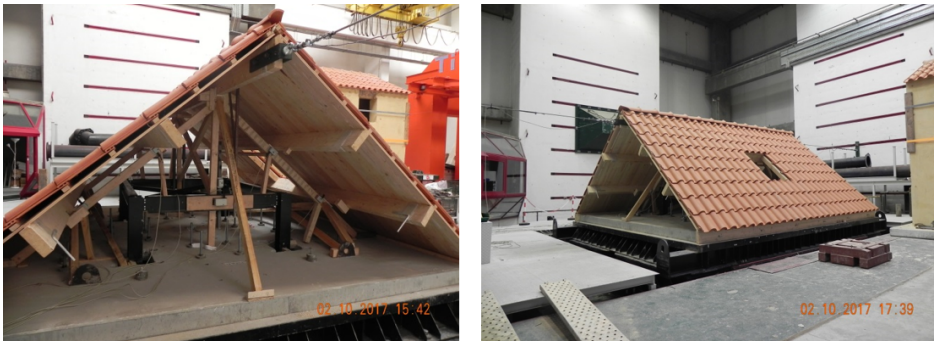

Figure 11 Support and guidance system (Correia et al., 2017)

5.2 Loading protocol and test specimen response

The roof was subjected to two full cycles at ±10 mm, ±50 mm, ±100 mm and ±150 mm. No particular damage was observed during the cyclic loading up to 150 mm, with the observed response being rather stable. As such, a decision was made to simply pushover the roof until failure would be reached, which happened for a displacement of 350 mm; the nails connecting the timber planks and the base beams were completely pulled out.

Figure 12 Damage observed during the final loading stage (Correia et al., 2017)

5.3 Numerical model

Although the roof cyclic test was carried out after the shake-table testing of the complete substructure, given that both sets of experimental results were rendered available in essentially simultaneous fashion (since the cyclic test came right after the shake-table one), both of the modelling endeavours were carried out in tandem. As such, the numerical modelling approach for the roof alone was naturally identical to what has been already described for the complete substructure (Section 4.1), with the obvious exception of the gable walls, which in this case are absent.

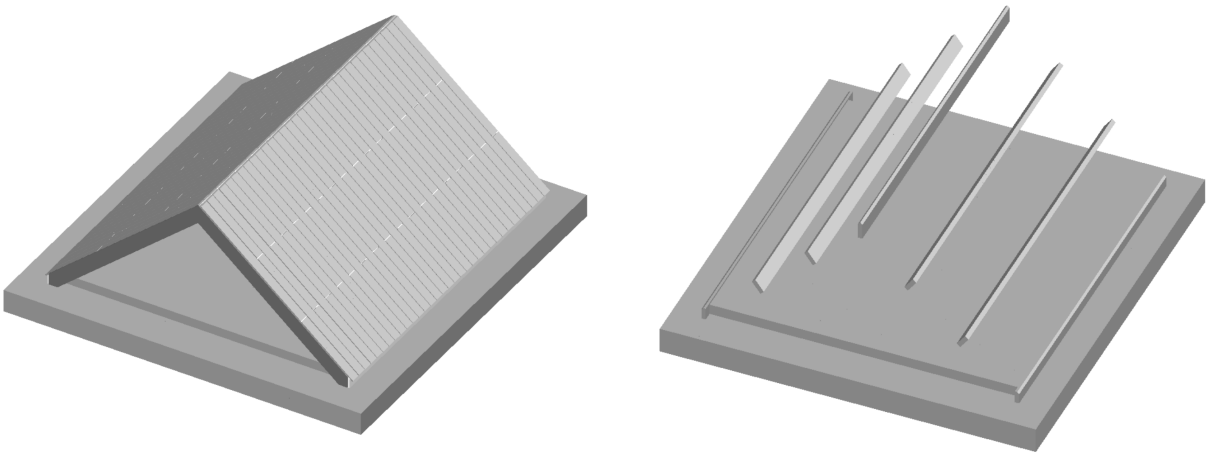

Figure 13 Screenshots of the numerical model

5.4 Hysteresis curves

A comparison between the numerical and experimental hysteretic response in terms of floor displacement (i.e. total "base" shear [kN] vs. attic floor horizontal displacement relative to the base [mm]) is show in the plots below, where grey stands for experimental recordings and black is numerical results.

Somewhat not unexpectedly, given the good performance of the complete substructure model reported already in Section 4.4, it can be observed that the roof model is able to adequately capture the cyclic response of the roof specimen.

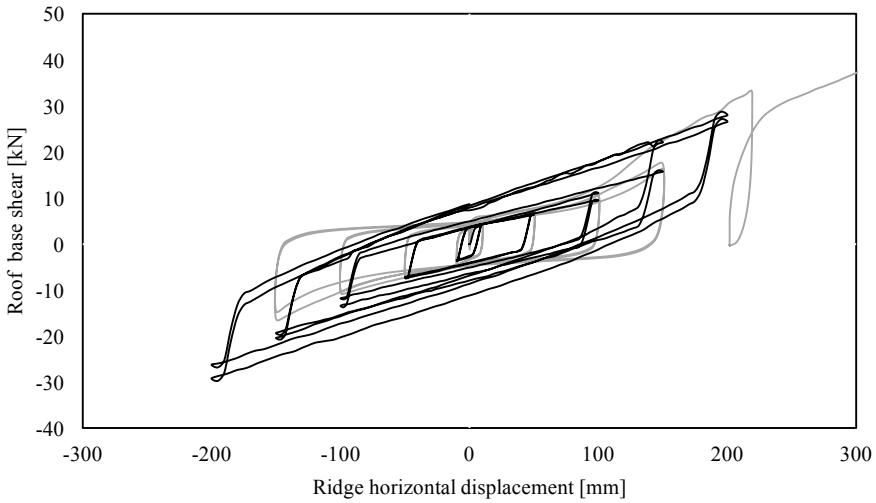

Figure 14 Experimental vs. numerical hysteresis curve

6 Closing Remarks

In this endeavour, the numerical modelling of a terraced house roof substructure was undertaken both prior and after its shake-table testing. The structure was composed of two URM gables (on one side a single leaf wall, on the other a cavity wall) made of CS and CL brick masonry, whilst the flexible diaphragm was constituted by longitudinal wooden beams covered by 2 cm thick plank elements. Following the collapse of the gable walls, the timber roof alone was also subjected to a quasi-static cyclic and pushover loading protocol.

The blind prediction modelling of this substructure highlighted the importance of QA'ing numerical models, as a basic error in the definition of the foundation boundary conditions led to a significant overestimation of the stiffness of the structure. In addition, the post-test availability of experimental data on the cyclic behaviour of the timber roof alone allowed the calibration of the model for this component of the complete substructure, which in turn then permitted the attainment of accurate estimations of the dynamic response and collapse mode of the test specimen.

Notwithstanding the good outcome of this modelling endeavour, it is felt that it could nonetheless be opportune to develop an alternative and more simplified manner in which to model the timber roof, in order to reduce the computational burden of running models such as the one used herein, where each member of the roof, including nailed connections, is explicitly modelled. As such, future work will focus on the adequate calibration of an equivalent membrane element to model this type of roofs.

References

ASI (2017) *Extreme Loading for Structures v5*, Applied Science International LLC., Durham (NC), USA.

Arup (2017) "LNEC-BUILD-1: Modelling Predictions and Analysis Cross Validation," *Report n. 229746_031.0_REP2004*, Amsterdam, The Netherlands.

Brignola, A., Podestà, S., Pampanin, S. (2008) "In-plane stiffness of wooden floor" *Proceedings of the New Zealand Society for Earthquake Engineering Conference*, Wellington, New Zealand.

Brooks J.J., Baker A. (1998) "Modulus of elasticity of masonry" *Masonry International*, Vol. 12, No. 2, pp. 58–63.

Ciesielski R. (1999) "The dynamic module of elasticity of brick walls," *Proceedings of the Conference of the Committee of Civil Engineering PZITB*, Lublin, Poland.

Correia AA., Tomassetti U., Graziotti F., Marques AI., Bernardo V. (2017) "Shake table test up to collapse on a roof substructure of a Dutch terraced house" European Centre for Training and Research in Earthquake Engineering (EUCENTRE), Pavia, Italy.

Graziotti F., Tomassetti U., Rossi A., Kallioras S., Mandirola M., Cenja E., Penna A., Magenes G. (2015) "Experimental campaign on cavity-wall systems representative of the Groningen building stock," *Report n. EUC318/2015U*, European Centre for Training and Research in Earthquake Engineering (EUCENTRE), Pavia, Italy. Available from URL: http://www.eucentre.it/nam-project

ICBO (1991) *Uniform Building Code*, International Conference of Building Officials, USA.

Kim J.J., Reda Taha M. (2014) "Experimental and numerical evaluation of direct tension test for cylindrical concrete specimens," *Advances in Civil Engineering*, Vol. 2014, pp. 1-8.

Malomo (2018) "Scrutinising the applicability of the Applied Element Modelling in the modelling of URM structures subjected to earthquake loading," *PhD Thesis*, University of Pavia, Italy. To be Submitted.

Matysek P., Zbigniew J. (1996) "Analysis of factors affecting the modulus of elasticity of the walls," *Proceedings of the Conference of the Committee of Civil Engineering PZITB*, Lublin, Poland.

Meguro K., Tagel-Din H. (2000) "Applied Element Method for structural analysis: Theory and application for linear materials," *JSCE International Journal of Structural Engineering and Earthquake Engineering*, Vol. 17, No. 1, pp. 21–35.

Meguro K., Tagel-Din H. (2001) "Applied Element simulation of RC Structures under cyclic loading," *ASCE Journal of Structural Engineering*, Vol. 127, No. 11, pp. 1295-1305.

Meguro K., Tagel-Din H. (2002) "Applied Element Method used for large displacement structure snalysis," *Journal of Natural Disaster Science*, Vol. 24, No. 2, pp. 65-82.

Mosayk (2016) "Using the Applied Element Method to model URM walls subjected to in-plane cyclic shear-compression," Pavia, Italy.

Mosayk (2017) "Using the Applied Element Method to model the collapse shake-table testing of a URM cavity wall structure," Pavia, Italy.

Tomassetti U., Correia A.A., Graziotti F., Marques A.I., Mandirola M., Candeias P.X. (2017a) "Collapse shaking table test on a URM cavity wall structure representative of a Dutch terraced house," European Centre for Training and Research in Earthquake Engineering (EUCENTRE), Pavia, Italy. Available from URL: http://www.eucentre.it/nam-project

Tomassetti U., Kallioras S., Graziotti F., Correia A. (2017b) "Final report on the construction of the building prototype at the LNEC laboratory," European Centre for Training and Research in Earthquake Engineering (EUCENTRE), Pavia, Italy.

Appendix A – further details on URM model building in ELS

This Appendix is common to a series of reports by Mosayk (2017a, 2017b, 2017c) concerning the modelling of the shake-table testing of a number of URM full-scale specimens (EUC-BUILD1, EUC-BUILD2, LNEC-BUILD1 and LNEC-BUILD2), and aims at providing further details on the modelling of:

- Contact surfaces between elements (mortared or nailed)
- Timber planks (of slabs and roofs)
- Connectors, ties and steel anchors

In addition, the procedure to derive mortar elastic properties by means of homogenisation formulae is also reported.

A.1 AEM modelling of contact surfaces between elements

According to the AEM, the connection between rigid bodies is assured by interface springs. Each contact surface, indeed, is characterised by a user-defined number of springs in which both the material properties and the damping of the system are lumped.

The analysis accuracy is directly proportional to the number of springs as well as the mesh discretisation (i.e. the number of rigid bodies constituting the assembly). In most cases the default value of 25 springs per contact surface is sufficient to represent adequately the actual behaviour of a given structural elements both in static and dynamic range. However, when the numerical model requires a refined discretisation (i.e. a larger number of elements), then if the contact surface is sufficiently small, the amount of interface springs can be reduced consistently, so as to reduce the computation burden. In the analyses presented in this report, indeed, 9 springs per contact surface (of the discretised elements) were employed, given that this proved to constitute a good compromise between accuracy and computational demand.

As depicted in Figure A.1, the springs are located at specific contact points and distributed uniformly along the contact surfaces, representing the stress/strain state of a given volume DV (or DA in 2D), as well as the contact stiffness. This modelling approach thus readily allows assigning equivalent mechanical properties to the contacts in order to describe the actual behaviour of a wide range of connections between different elements (e.g. nailed, welded or interlocking connections).

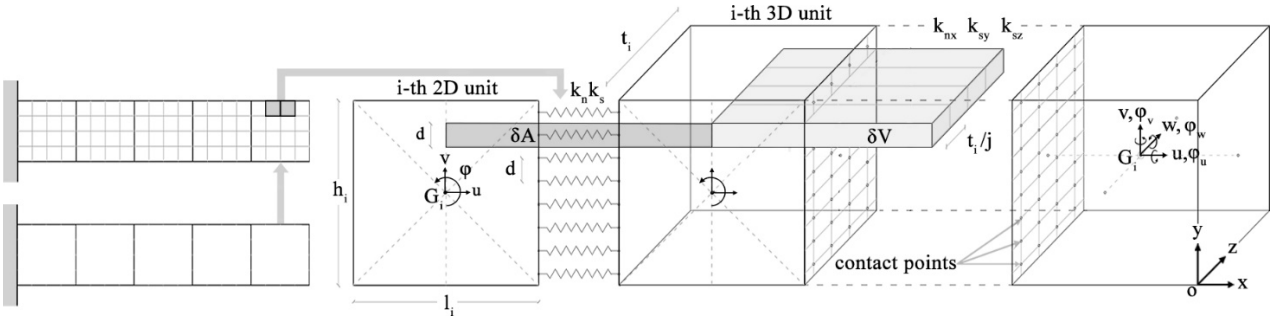

Figure A.1 Multi-scale discretization of both 2D and 3D rigid body assembly

In Figure A.2, below, the different types of contact connections considered in this modelling endeavour (which, it is reiterated, concerned the modelling of the shake-table testing of the four URM full-scale specimens listed above, not all of which are described in this one report) are shown.

(a) (b) (c) (d)

Figure A.2 L-shaped anchors (a), RC slab/beam connection (b), pure frictional contact between walls and planks (c) and nailed connections between boards and ridge/timber plate (d) (Correia et al., 2017)

A.1.1 Nailed connections between beam and plank elements

The mechanical connection between wooden boards and beams in traditional flexible diaphragms, is often provided by one or more steel nails distributed along the contact surface (Brignola et al., 2008) as reported in Figure A.3 below.

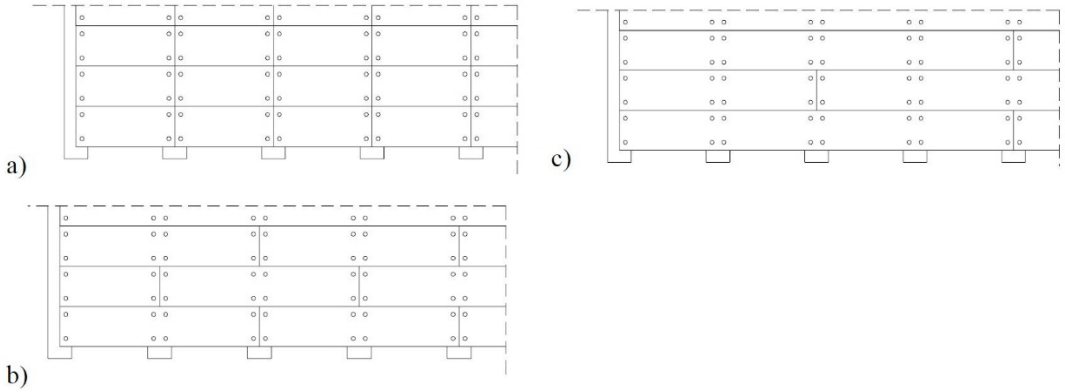

Figure A.3 Types of common nailed connections between beams and boards (Brignola et al., 2008)

The stiffness related to these interfaces are calibrated from the force-slip behaviour of the nail ($k_{ser} = F'/d'$), assuring the actual shear deformability to the connection. According to Eurocode 5 (2004), the slip modulus of a nail with diameter d' can be evaluated by means of Eq. (A.1) below, considering the simplified elastic-perfectly plastic response depicted in Figure A.4. Thus, considering a contact area A_c between board and beam, the following equivalent shear modulus Geq_{nails}, reported in Eq. (A.2) can be introduced and subsequently assigned to the related interface, where L represents the distance from the centroids of elements.

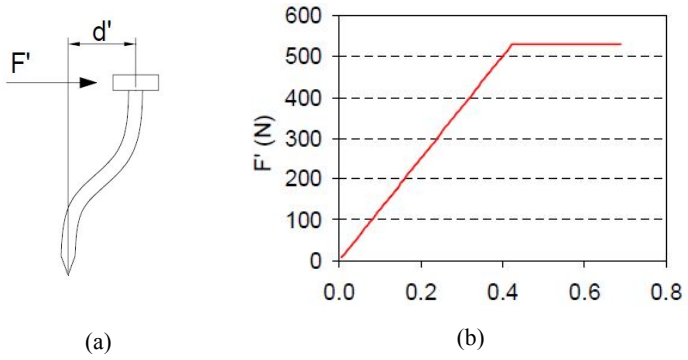

(a) (b)

$$\boldsymbol{k_{ser} = \left(\frac{\rho^{1.5} \times d'^{0.8}}{30}\right)} \quad \text{(A.1)}$$

$$Geq_{nails} = \frac{Kser \times L}{2 \times A_c} \quad \text{(A.2)}$$

Figure A.4 Nail slip behaviour (a), and its force-displacement bilinear response (b) (Brignola et al., 2008)

With the aim of investigating the numerical response of this type of connection, several simplified models, of the type illustrated below in Figure A.5, were elaborated. In Table A.1 the main equivalent modelling parameters concerning the simplified model (compatible with the roof structure of both EUC-BUILD1, LNEC-BUILD1 and LNEC-BUILD2) are reported, whereas the associated force-displacement curve is depicted in Figure A.5(c).

Table A.1 Mechanical properties assigned to the simplified model

Simplified model subjected to pure shear loading conditions			
Material model	Bilinear material	Equivalent yield stress [MPa]	4
Beam height [mm]	220	Number of nails [-]	1
Board thickness [mm]	20	K_{ser} [N/mm]	965
Distance L between centroids [mm]	120	Yield force [N]	576
Area of contact [mm^2]	14400	Yield displacement [mm]	0.77
Nail diameter [mm^2]	4	Eeq_{nail} [MPa]	11
Poisson coefficient [-]	0.25	Geq_{nail} [MPa]	4.4

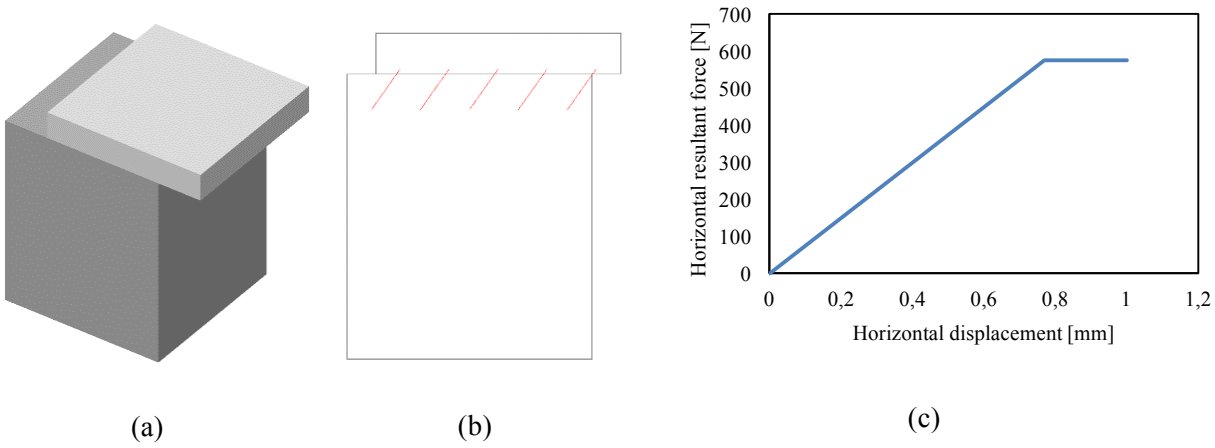

(a) (b) (c)

Figure A.5 Screenshot of the model (a), equivalent spring layer representing the nailed connection (b) and force-displacement plot (c)

In the abovementioned model, the base (beam) was fully fixed, whereas the upper element (plank) was free to move in the horizontal direction only. Hence, the interface springs were subjected to pure shear. With a view to account for the rotational deformability as well, the elastic modulus of the nail was inferred by multiplying Geq_{nail} by a factor of 2.5, yielding the typical constitutive equation for isotropic materials (Lekhnitskii, 1963).

However, further improvements related to the latter aspects are needed. Since the yield stress can be reached both in tension and in pure shear, the preliminary modelling results obtained for LNEC-BUILD1 using this methods prior the shake-table test, for instance, have shown that an early tensile failure of the connection (reached due to the increase in the rotation demand due to the relative displacement of adjacent boards) might occur.

Hence, small variations of this approach have been employed and applied for the subsequent models. For EUC-BUILD1, EUC-BUILD2, LNEC-BUILD1 and LNEC-BUILD2 (post-test refined simulations), indeed, the equivalent yield stress was increased consistently to avoid the early rotational failure of the beam-plank interface, as reported in Table A.2. This effectively rendered the updated contact surface as featuring an equivalent elastic interface, limited by the actual shear stiffness of the nail.

Table A.2 Mechanical properties of the nailed connection for EUC-BUILD2, LNEC-BUILD1 and LNEC-BUILD2

LNEC-BUILD1 (blind prediction model)			
Material model	Bilinear material	Equivalent yield stress [MPa]	4
Beam height [mm]	220	Number of nails [-]	2
Board thickness [mm]	20	K_{ser} [N/mm]	965
Distance L between centroids [mm]	120	Yield force [N]	---
Area of contact [mm^2]	14400	Yield displacement [mm]	---
Nail diameter [mm^2]	4	Eeq_{nail} [MPa]	22
Poisson coefficient [-]	0.25	Geq_{nail} [MPa]	8.8
EUC-BUILD1, LNEC-BUILD1, LNEC-BUILD2 (post-test refined models)			
Material model	Bilinear material	Equivalent yield stress [MPa]	360
Beam height [mm]	220	Number of nails [-]	2
Board thickness [mm]	20	K_{ser} [N/mm]	965
Distance L between centroids [mm]	120	Yield force [N]	---
Area of contact [mm^2]	14400	Yield displacement [mm]	---
Nail diameter [mm^2]	4	Eeq_{nail} [MPa]	22
Poisson coefficient [-]	0.25	Geq_{nail} [MPa]	8.8
EUC-BUILD2			
Material model	Bilinear material	Equivalent yield stress [MPa]	360
Beam height [mm]	180	Number of nails [-]	40[1]
Board thickness [mm]	24	K_{ser} [N/mm]	965
Distance L between centroids [mm]	102	Yield force [N]	---
Area of contact [mm^2]	410000[1]	Yield displacement [mm]	---
Nail diameter [mm^2]	4	Eeq_{nail} [MPa]	13
Poisson coefficient [-]	0.25	Geq_{nail} [MPa]	5

[1] referred to the average contact area between a single transverse frame and the equivalent membrane element

A.1.2 Definition of "weak" and "cracked" mortar spring interfaces

In some cases (i.e. the modelling of EUC-BUILD1 and LNEC-BUILD1, post-test refined model) the connection between the lateral timber beam of the wooden roof structure, the RC slab and the URM cavity-wall system was characterised by peculiar mechanical properties. Indeed, the connection between the RC slab and the lateral timber beam of both EUC-BUILD1 and LNEC-BUILD1 consisted in a series of threaded bars (Graziotti et al., 2015), with the RC slab being then bonded to the transverse CS walls, while the beam is connected by means of a mortar layer to the CL brick masonry transverse walls.

Noteworthily, and also as gathered from Figure below, for both the specimens the gap between the RC slab and the longitudinal walls was filled after the temporary supports removal (i.e. after RC slab deflection); since the connection between these elements was provided only by this mortar layer, a "weak" spring interface was adopted, with a very low flexural and shear stiffness.

Further, in the case of LNEC-BUILD1, with aim to take into account the damage occurred at the interface between the RC slab and the lateral during transportation phases (Tomassetti et al., 2017), a "cracked" mortar spring interface has been introduced. This layer has almost zero flexural and shear stiffness, zero tensile and shear strength, and a compressive strength equal to the one of the brick.

(a) (b)

Figure A.6 Constructional details of the gap between CL walls/timber beam (a) and CS walls/RC slab (b) (Graziotti et al., 2015)

A.2 Numerical modelling of plank elements

The overall diaphragm flexibility can be evaluated by analysing the contribution to the in-plane deformation of the timber floor separately, as suggested by Brignola et al. (2008). In this sense, three different deformability contributions are distinguished: the flexural deformation of the single board, shear deformation of the single board and the rigid rotation of the board due to nails slip (see Figure A.7).

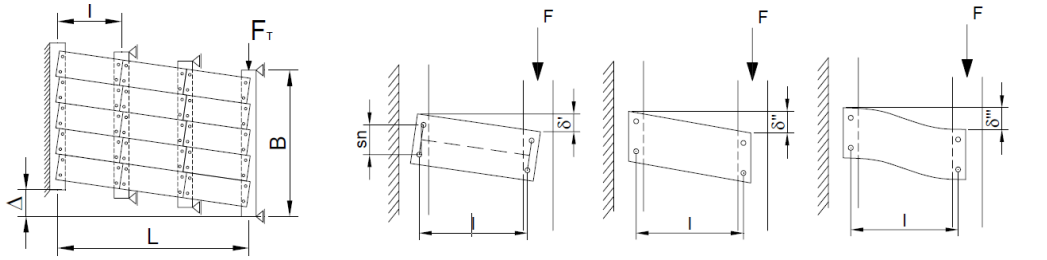

(a) (b) (c) (d)

Figure A.7 Deformability contributions of a given flexible diaphragm (Brignola et al., 2008)

Thus, it is possible to define an equivalent shear modulus that combines the three contributions of flexibility according to Eq. (A.3), where X is the shear factor, G shear modulus of planks, E flexural modulus parallel to grain of planks, A board section, I moment of inertia of plank section and s_n is the wheelbase between beams. Moreover, this result obtained for one board can be extended to the whole diaphragm when the wood planks are interrupted at each beams, as noted by Brignola et al. (2008).

$$\boldsymbol{Geq_{plank}} = \left(\frac{\boldsymbol{X}}{\boldsymbol{A}}\right)\left(\frac{\boldsymbol{l}}{\boldsymbol{k_{ser}s_n^2}} + \frac{\boldsymbol{X}}{\boldsymbol{GA}} + \frac{\boldsymbol{L}}{\boldsymbol{12EI}}\right)^{-1} \tag{A.3}$$

However, since the deformability of nails is already accounted by the spring interface described in the previous sub-section, Eq. (A.4) can be simplified as follows:

$$\boldsymbol{Geq_{plank}} = \left(\frac{\boldsymbol{X}}{\boldsymbol{A}}\right)\left(\frac{\boldsymbol{X}}{\boldsymbol{GA}} + \frac{\boldsymbol{L}}{\boldsymbol{12EI}}\right)^{-1} \tag{A.4}$$

Two main modelling strategies have been employed for modelling the roof structures of the URM full-scale specimens mentioned above, due to different construction details. Indeed, the roof of EUC-BUILD1, LNEC-BUILD1 and LNEC-BUILD2 was a relatively simple bearing system,

constituted by longitudinal beams covered by transverse boards and tiles (see Figure A.8). The roof of EUC-BUILD2, instead, was formed by a series of wooden frames supporting the planks and tiles assembly. Furthermore, the gable structure required specific constructional details, as described in the related report (Graziotti et al., 2016).

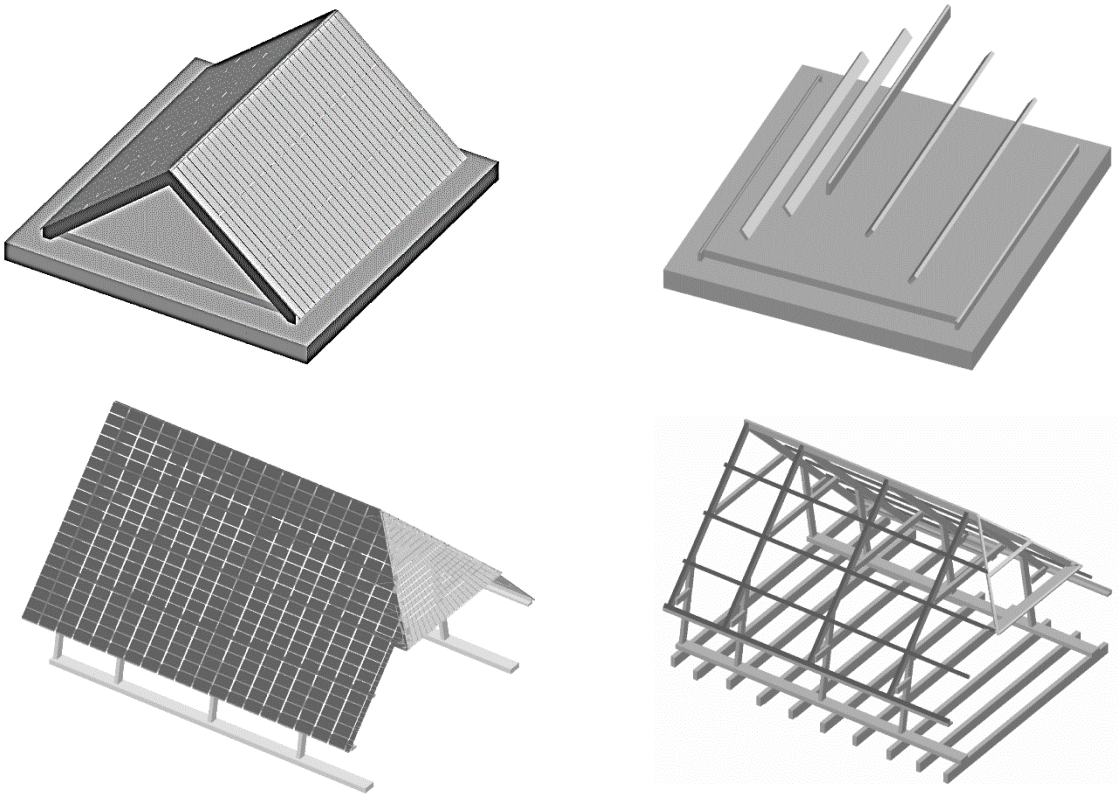

Figure A.8 Roof structure of LNEC-BUILD2 (above) and EUC-BUILD2 (below)

Hence, in case of EUC-BUILD1, LNEC-BUILD1 and LNEC-BUILD2 each plank was modelled separately, resulting in a more accurate numerical response, whereas the planks of EUC-BUILD2 were modelled as an equivalent continuous membrane with the aim of reducing the computational burden and the modelling efforts. The latter approach, as it is clearly observable from the results shown in the corresponding report, still requires further enhancements.

In Table A.3, the main numerical parameters, inferred using Eq. (A.4) and subsequently employd for the modelling of the abovementioned full-scale specimens, are briefly summarised:

Table A.3 Plank material properties employed for the modelling of for EUC-BUILD2, LNEC-BUILD1 and LNEC-BUILD2

LNEC-BUILD1 (blind prediction model)			
Geometrical parameters		Inferred values	
Board thickness	20 mm	Shear factor	1.2
Board width	180 mm	Shear deformation of the single board	8e-07 m/N
Elastic modulus of wood	12000 MPa	Deformability due to rigid rotation of the board	5.18e-0.5 m/N
Shear modulus of wood	750 MPa	Flexural deformation of the single board	4.16e-06 m/N
Board Length	1.8 m	Equivalent shear modulus Geq_{plank}	120.80 MPa
EUC-BUILD1, LNEC-BUILD1, LNEC-BUILD2 (post-test refined models)			
Board thickness	20 mm	Shear factor	1.2
Board width	180 mm	Shear deformation of the single board	8e-07 m/N

Elastic modulus of wood	12000 MPa	Deformability due to rigid rotation of the board	5.18e-0.5 m/N
Shear modulus of wood	750 MPa	Flexural deformation of the single board	4.16e-06 m/N
Board Length	1.8 m	Equivalent shear modulus Geq_{plank}	120.80 MPa
EUC-BUILD2			
Board thickness	18 mm	Shear factor	1.2
Board width	150 mm	Shear deformation of the single board	2.67e-06 m/N
Elastic modulus of wood	5000 MPa	Deformability due to rigid rotation of the board	7.43e-05 m/N
Shear modulus of wood	333 MPa	Flexural deformation of the single board	2.63e-05m/N
Board Length	2.0 m	Equivalent shear modulus Geq_{plank}	22.98 MPa

A.3 Connectors, ties and steel anchors elements

The use of metal reinforcements and connectors, such as ties and L-shaped anchors (see Figure A.9), is a relatively common practice in the construction of URM buildings in the Groningen area. These elements, as confirmed also by experimental tests on structural sub-components (Graziotti et al., 2015), strongly affect the behaviour of URM constructions. In Figure A.10 the modelling of the ties elements and the L-shaped steel anchors for EUC-BUILD1 and LNEC-BUILD1 is shown.

(a) (b) (c)

Figure A.9 RC slab/beam connection (a), steel ties (b) and L-shaped anchors (c) (Correia et al., 2017)

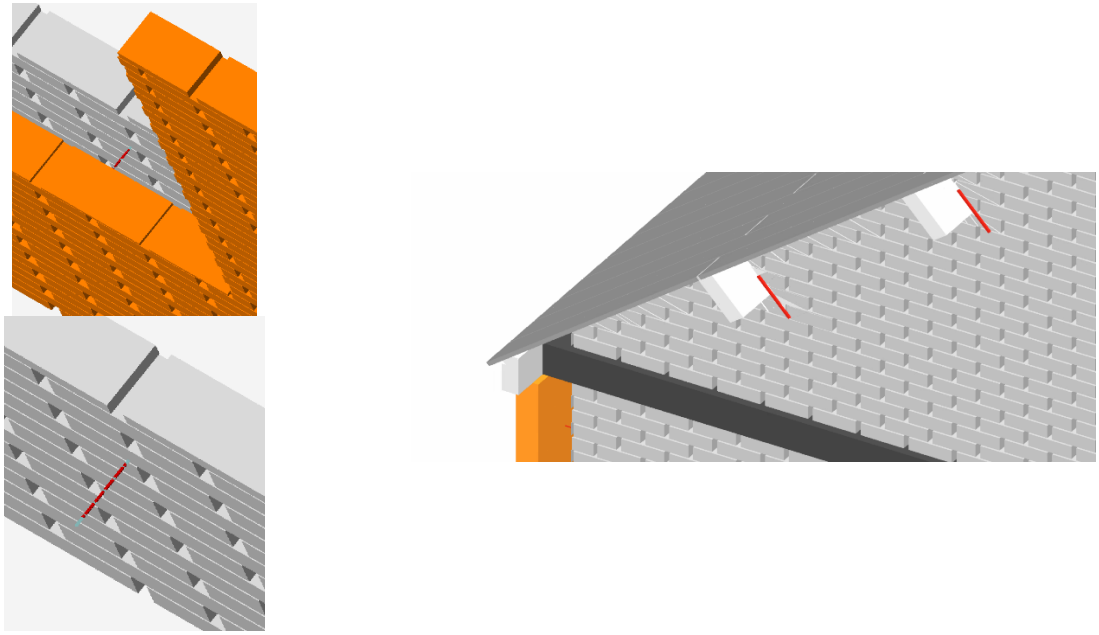

(a) (b)

Figure A.10 Nails connections of EUC-BUILD1 (a) and L-shaped anchors of LNEC-BUILD1 (b)

As mentioned above, the connectors between the RC slab and the lateral timber beams were made of threaded bars (diameter of 10 mm). The steel ties connecting the CS to the CL brick masonry walls were instead characterised by a diameter of 3.4 mm, whereas the L-shaped steel anchors (diameter of 15 mm) assured the connection between the timber beam extremities and the gables.

The RC slab/lateral timber beam connector was modelled as an equivalent elastic spring interface, avoiding spurious relative displacement not observed during the tests, whereas both the L-shaped anchors and the ties were modelled by means of three-dimensional beam elements.

In Table A.4, the constitutive models and the most relevant mechanical properties are briefly summarised:

Table A.4 Constitutive models and mechanical properties of metal connectors and anchors

EUC-BUILD1, LNEC-BUILD1, LNEC-BUILD2			
RC slab/lateral timber beams		L-shaped anchors and steel ties	
Material model	Elastic material	Material model	Bilinear material
Element type	Spring interface	Element type	3D girder
Young's modulus [MPa]	10000	Young's modulus [MPa]	210000
Shear modulus [MPa]	400	Shear modulus [MPa]	84000
Friction coefficient [-]	0.4	Friction coefficient [-]	0.8
Separation strain [-]	1e+08	Separation strain [-]	100

A.4 Derivation of mortar Young's modulus from homogenisation formulae

As extensively discussed in Mosayk (2016), since the Young's modulus for both the masonry panels assembly and the bricks are known (from material characterisation tests), the Young's modulus of the mortar can be computed by means of the equations reported in Table A.5, often employed to develop a homogenisation process (i.e. to estimate the Young's modulus of a masonry panel when in knowledge of the Young's moduli of its brick and mortar components).

All four equations described below, where ξ is the ratio of brick's height to the thickness of mortar joint, were used to infer E_{mo}, and then the ensuing average considered for the models. It is noted that when unrealistic values were obtained from a given equation, such values were not considered in computation of the average value.

Furthermore, it is noted that the shear modulus G_{mo} was obtained assuming $G = E/\big(2(1+\nu)\big) = 0.4E$ with $\nu = 0.25$, because no experimental data concerning this specific parameter was available.

Table A.5 Derivation of the Young's modulus of mortar through homogenization criteria

Reference	Homogenisation formulae		Reference	Homogenisation formulae	
Brooks et al. (1998)	$E_{mo} = \left(\frac{-4E_mE_b}{25E_m - 29E_b}\right)$	(A.5)	Matysek et al. (1996)	$E_{mo} = \left(\frac{E_mE_b}{E_b - 1.25\zeta(E_m - E_b)}\right)$	(A.6)
Ciesielski (1999)	$E_{mo} = \left(\frac{-E_mE_b}{5E_m - 6E_b}\right)$	(A.7)	ICBO (1991)	$E_{mo} = \left(\frac{E_mE_b}{\zeta(E_m - E_b) + E_b}\right)$	(A.8)

In the following Table A.6, the mortar Young's moduli and the mean values subsequently adopted for the modelling of the full-scale URM specimens are reported.

Table A.6 Mortar Young's modulus calculation for each full-scale specimen

LNEC-BUILD1 (blind prediction model)			
CS			
Reference	E_{mo} [MPa]	Reference	E_{mo} [MPa]
Brooks et al. (1998)	895	Matysek et al. (1996)	675
Ciesielski (1999)	1060	ICBO (1991)	1360
Mean value [MPa]			
997			
CL			
Reference	E_{mo} [MPa]	Reference	E_{mo} [MPa]
Brooks et al. (1998)	2927	Matysek et al. (1996)	2927
Ciesielski (1999)	3261	ICBO (1991)	Not reliable
Mean value [MPa]			
3039			
LNEC-BUILD1, LNEC-BUILD2 (post-test refined models)			
CS			
Reference	E_{mo} [MPa]	Reference	E_{mo} [MPa]
Brooks et al. (1998)	4626	Matysek et al. (1996)	3935
Ciesielski (1999)	5059	ICBO (1991)	Not reliable
Mean value [MPa]			
4537			
CL			
Reference	E_{mo} [MPa]	Reference	E_{mo} [MPa]
Brooks et al. (1998)	3184	Matysek et al. (1996)	3184
Ciesielski (1999)	4237	ICBO (1991)	Not reliable
Mean value [MPa]			
3039			
EUC-BUILD1			
CS			
Reference	E_{mo} [MPa]	Reference	E_{mo} [MPa]
Brooks et al. (1998)	4626	Matysek et al. (1996)	3935
Ciesielski (1999)	5059	ICBO (1991)	Not reliable
Mean value [MPa]			
4537			
CL			
Reference	E_{mo} [MPa]	Reference	E_{mo} [MPa]
Brooks et al. (1998)	Not reliable	Matysek et al. (1996)	Not reliable
Ciesielski (1999)	Not reliable	ICBO (1991)	Not reliable
Adopted value [MPa]			
4537 (equal to the one of the CS mortar)			
EUC-BUILD2			
CL			
Reference	E_{mo} [MPa]	Reference	E_{mo} [MPa]
Brooks et al. (1998)	4508	Matysek et al. (1996)	4508
Ciesielski (1999)	4805	ICBO (1991)	Not reliable
Mean value [MPa]			
4607			

A.5 References

Brignola, A., Podestà, S., Pampanin, S. (2008) "In-plane stiffness of wooden floor" *Proceedings of the New Zealand Society for Earthquake Engineering Conference*, Wellington, New Zealand.

Eurocode 5, "Design of timber structures", EN 1995-1-1 (2004)

Graziotti F., Tomassetti U., Rossi A., Kallioras S., Mandirola M., Cenja E., Penna A., Magenes G. (2015) "Experimental campaign on cavity-wall systems representative of the Groningen building stock," *Report n. EUC318/2015U*, European Centre for Training and Research in Earthquake Engineering (EUCENTRE), Pavia, Italy. Available from URL:

Graziotti F., Tomassetti U., Rossi A., Kallioras S., Mandirola M., Penna A., Magenes G. (2016) "Experimental campaign on a clay URM full-scale specimen representative of the Groningen building stock," *Report n. EUC128/2016U*, European Centre for Training and Research in Earthquake Engineering (EUCENTRE), Pavia, Italy. Available from URL: http://www.eucentre.it/nam-project

Lekhnitskii S.G., Fern P. (1964) "Theory of Elasticity of an Anisotropic Elastic Body," *Physics Today*, Vol. 17, No. 1, p. 84.

Mosayk (2016) "Using the Applied Element Method to model URM walls subjected to in-plane cyclic shear-compression," Pavia, Italy.

Mosayk (2017a) "Using the Applied Element Method to model the shake-table testing of two full-scale URM houses," Pavia, Italy.

Mosayk (2017b) "Using the Applied Element Method to model the collapse shake-table testing of a URM cavity wall structure," Pavia, Italy.

Mosayk (2017c) "Using the Applied Element Method to model the collapse shake-table testing of a terraced house roof substructure," Pavia, Italy.

Tomassetti U., Kallioras S., Graziotti F., Correia A. (2017b) "Final report on the construction of the building prototype at the LNEC laboratory," European Centre for Training and Research in Earthquake Engineering (EUCENTRE), Pavia, Italy.